Latest Developments in Suspension and Liquid Precursor Thermal Spraying

Pierre Fauchais and Ghislain Montavon

(Submitted April 23, 2009; in revised form September 9, 2009)

The interest to manufacture onto large surfaces thick (i.e., 10-20 μm, average thickness) finely structured or nanostructured layers is increasingly growing since the past 10 years. This explains the interest for suspension thermal spraying (STS) and solution precursor thermal spraying (SPTS), both allowing manufacturing finely structured layers of thicknesses varying between a few micrometers up to a few hundreds of micrometers. STS aims at processing a suspension of sub-micrometer-sized or even nanometer-sized solid particles dispersed in a liquid phase. The liquid phase permits the injection of particles in the thermal flow (i.e., due to their size, a carrier gas cannot play this role). SPTS aims at processing a solution of precursors under the same conditions. Upon evaporation of the liquid phase, the precursor concentration increases until precipitation, pyrolysis, and melting of small droplets occur. Compared to conventional thermal spray routes, STS and SPTS are by far more complex because fragmentation and vaporization of the liquid control the coating build-up mechanisms. Numerous studies are still necessary to reach a better understanding of the involved phenomena and to further develop the technology, among which are injection systems, suspension and solution optimizations, spray kinematics, etc. This review presents some recent developments and our present knowledge in this field together with the available tools implemented to characterize the plasma-liquid interaction and the coating formation.

1. Introduction

Nano-composite materials, in particular ceramics, made of at least one phase at the nanometer scale, have been intensively studied during these last years. Their interest relies in their improvement in strength, reduction of micro-cracking, better resistance to thermal shock, and low wear. However, processing of nano-sized particles is not simple as underlined in the review of the different processes by Viswanathan et al. (Ref 1). Among the possible processes, thermal spray seems to be very promising (Ref 2) to achieve nano- or at least finely

structured materials due to the rapid solidification rate, opening the way to prepare advanced materials with unique properties.

In fact, two routes can be implemented to reach this goal: spraying micrometer-sized particles as in conventional thermal spraying or spraying sub- or nanometer-sized particles using a liquid carrier instead of gas (Ref 3).

With conventional spraying (sizes in the tens of micrometer range):

- Spraying particles made of agglomerated nanometer-sized particles [see the review of Lima and Marple (Ref 4)] by operating spray systems in relatively narrow spray windows [with only particles partial melting (Ref 5)].
- Spraying specialized iron-based compositions (6-7 different components) with a low critical cooling rate (10^4 K s^{-1}) for metallic glass formation. A primarily amorphous structure is formed and, after a heat treatment above crystallization temperature, the coating is densified into a multiphase nano-composite microstructure (Ref 6, 7).

With liquid carrier (injected as jet or drops), to which this paper is exclusively devoted, two routes can also be implemented with the liquid containing:

- Precursors in solution (Ref 3, 8) or in sol-gel colloidal solution (Ref 9).
- A suspension of nanometer- or sub-micrometer-sized particles (Ref 3, 10).

The following will be presented successively: (i) the equipments: spray torches, solution and suspension

Pierre Fauchais and **Ghislain Montavon**, Faculty of Sciences and Technologies, University of Limoges, SPCTS, UMR CNRS 6638, 123 Avenue Albert Thomas, 87060 Limoges cedex, France. Contact e-mails: fauchais@unilim.fr and ghislain.montavon@unilim.fr.

preparation, injection systems, and process characterizations; (ii) the interaction between the liquid stream and the hot gas flow (produced by direct current plasma torches or combustion torches); (iii) the coating formation and in-flight particles/hot gas flow interactions, the resulting spray beads, the spray pattern and the coatings structure; (iv) the most studied coatings: yttria-partially stabilized zirconia, alumina, alumina-titania, chromia, glass, and hydroxyapatite.

2. Equipments

2.1 Spray Guns

2.1.1 General Remarks. Liquid injection results in stream or droplets fragmentation before resulting in droplet vaporization. In plasma flows, this vaporization followed by the transformation of vapor into plasma drastically cool them down even if the liquid is combustible. The combustion can occur only far downstream of the nozzle exit where the air entrainment is sufficiently important. With combustion flames, such as HVOF (high-velocity oxy-fuel spray) where the combustion is fuel lean, the excess of oxygen permits the combustion of the liquid, especially when it is injected axially directly into the combustion chamber.
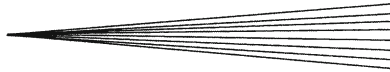
Spray torches must achieve high flow velocities in order to sufficiently accelerate particles which, otherwise, due to their low mass, follow the impacting flow parallel to the substrate surface without impacting the substrate. This phenomenon is controlled by the Stokes number that must be higher than 1 and is defined by:

$$S_t = \frac{\rho_p d_p^2 v_p}{\mu_g \ell_{BL}} \tag{Eq 1}$$

where the indexes p and g are related to the particles and gas, respectively, ρ being the specific mass (kg m^{-3}), d the diameter (m), v the velocity (m s^{-1}), μ the molecular viscosity (Pa·s) and ℓ_{BL} the thickness of the flow boundary layer in front of the substrate (m). For example, with an Ar-H$_2$ plasma, $S_t = 1$ for $v_p = 300$ m s^{-1} and $d_p = 0.3$ μm.

2.1.2 Plasma Torches. Different types of torches are used:

- The conventional torches with a stick-type cathode and 30-40 kW power levels working with Ar-H$_2$, Ar-He, or Ar-H$_2$-He plasma forming gas mixtures. Though hydrogen provides an excellent heat transfer, it also induces very high arc root fluctuations resulting in large voltage fluctuations, i.e., the mean fluctuation amplitude ΔV relative to the time averaged voltage $\bar{V}$ is greater than unity $\left(\Delta V/\bar{V} > 1\right)$. On the contrary, Ar-He mixture results in $\Delta V/\bar{V} < 0.25$ (Ref 10).

- The Triplex torch (Sultzer-Metco, Wohlen, Switzerland) with 70-80 kW power levels working with Ar, Ar-He, or Ar-N$_2$ plasma gas mixtures. From the three cathodes and three independent electric sources result three arcs striking at a unique anode separated by insulating rings (so-called neutrode) permitting the generation of longer electric arcs compared to conventional stick-type cathode plasma torches. Mean voltages can reach 100-120 V with Ar-He plasma instead of less than 40 V with conventional torches. Thus, if ΔV is still about 10 V, the $\Delta V/\bar{V}$ ratio is below 0.1. This system has been used to spray suspensions (Ref 11).

- The Axial III torch (Mettech, Vancouver, Canada) with three cathodes and three anodes operated by three power supplies. The three plasma jets converge within an interchangeable nozzle and liquid feedstock is injected axially between the three plasma jets (Ref 12, 13).

2.1.3 HVOF Torches. Torches with axial injection such as DJ2700 (Sulzer-Metco, Wohlen, Switzerland) (Ref 12) or Top-Gun (GTV, Düsseldorf, Germany) (Ref 14, 15) are used. When the suspension is made of water, poor coatings are obtained due to insufficient flame enthalpy. Much better results are obtained with ethanol, but even a low percentage of water in ethanol drastically cools the flame. Injecting combustible liquids raises the combustion chamber pressure, resulting in instabilities in the acetylene flow (acetylene-oxygen giving the highest combustion temperature). Thus, propane and ethane are used (Ref 15) to achieve stable flames with the Top-Gun system while Oberste-Berghauss et al. (Ref 12) have chosen propylene with the DJ2700 system.

2.2 Suspension and Solution Preparation

2.2.1 General Remarks. The injection of a liquid as a continuous stream or drops is a very complex phenomenon because upon penetration into the hot gas flow, fragmentation and vaporization occur. Fragmentation, depending on the Weber (We) and Ohnesorge (Oh) numbers (Ref 3), can be partially tailored by adjusting the liquid surface tension, σ_l, and the viscosity, μ_l. Though using water instead of ethanol increases σ_l by a factor of about 2, it also requires more than double the energy to vaporize water (Ref 3). Water is mainly used to produce yttria-partially stabilized zirconia (Y-PSZ) coatings from aqueous salts containing zirconium and yttrium [solution precursor thermal spraying (SPTS)]. The concentration of precursors produces modest changes in the solution specific mass and surface tension, but large changes in the solution viscosity (Ref 16).

For suspensions, the mostly used liquid phases are ethanol and water. Different products can be added to the liquid phase to modify its surface tension and/or its viscosity (Ref 17, 18). Raising the suspension content in weight fraction of particles increases the suspension viscosity. The particles sedimentation is impeded or strongly delayed by using a dispersant, which nature and quantity must be optimized (Ref 3, 17). The pH adjustment is also an important factor to be taken into consideration. Particles with size distributions in the nanometer or submicrometer ranges are now available on the market. Though the oxide suspensions are rather easy to stabilize,

it is more difficult with a cermet such as WC-Co. This is due to the high specific density of WC-Co powders and the widely different acid/base properties of the two main particle constituents (Ref 12).

A zirconia sol can be prepared by neutralization of zirconium oxy-chloride in an aqueous media followed by hydrothermal crystallization (Ref 9). When heating the mixture in a container at a minimum temperature of 170 °C for 20 h at a minimum pressure of 2 MPa, a precipitation of crystalline oxide occurs. The precipitate is a mixture of monoclinic and tetragonal phases and it is washed to get rid of the excess ammonium hydroxide. The particles are then suspended in water by addition of hydrochloric acid (pH 3).

2.2.2 Liquid Injection. Two main routes can be implemented for liquid injection in the hot gas flow: atomization or mechanical injection.

Two-phase atomizers (liquid-gas) are extensively used (Ref 3, 8, 17-24). Conventional atomizers produce droplets with a wide size distribution as well as wide spray angles as high as 60°. It is clear that the distribution must be the narrowest possible to control the interaction between the hot gas flow and the liquid, as shown in next section. Moreover, the external dimensions of these atomizers can be in the range of 20 to 30 mm, which makes the injection close to the spray torch nozzle exit difficult. It is also necessary to adapt the droplet velocity for adequate penetration into the hot gas flow, especially when considering radial injection. Atomizers with rather narrow particle size distribution and spray cone have been developed by Kassner et al. (Ref 11) and Jordan et al. (Ref 24).

For mechanical injection, the most encountered technological routes are mainly (i) pressurized reservoirs with plasma torches (Ref 3) and HVOF (Ref 14, 15). Typical nozzle internal diameters (i.d.) are in the few hundreds of micrometers range (e.g., 300 μm). The drawback is that the injection pressure varies as the 4th power of the reverse of injector i.d., for the same liquid flow rate. Indeed, for i.d. = 50 μm, the pressure should be 40.5 MPa versus 6 MPa for i.d. = 300 μm. (ii) A magnetostrictive rod is disposed at the backside of the nozzle to superimpose pressure pulses at variable frequencies (up to a few tens of kHz) (Ref 13), which is the principle of ink jets printers (Ref 25).

2.3 Diagnostics

The liquid jet (outside the nozzle) can be visualized by illuminating it with a laser shot and recording the image with a CCD camera that has a fast shutter (a few tens of microseconds). As the laser shot is short (a few microseconds), it has to be triggered by the voltage fluctuations (Ref 26). Such systems (Ref 3, 26) give information about liquid penetration and fragmentation. By superposing several images taken in the same conditions and filtering them adequately, it becomes possible to determine the deviation angle of the liquid stream together with the dispersion of fragmented drops and droplets (Ref 26). More precise information, such as droplet velocities, can

be obtained by using a shadowgraph technique based on pulsed back light illumination of the liquid material (Ref 27). However, the minimum droplet size which can be discriminated depends upon the number of pixels of the camera and are generally in the range of a few tens of micrometers (that corresponds to the smallest droplets that can be distinguished and hence analyzed).

Particle velocities and temperatures can be also measured in-flight (downstream of the jet core) using the Accuraspray Diagnostic System (Tecnar, Saint Bruno, Canada) (Ref 13).

Particles and/or lamellae can be collected in-flight on a substrate fixed at the extremity of a pendulum crossing rapidly (at about 1 m s^{-1}) the hot gas flow at different distances downstream of the nozzle exit.

Particles and/or lamellae can be also collected on a substrate, disposed at the spray distance, protected by a water-cooled shield which can be opened for a few tenths of seconds (Ref 3). To enlarge the collecting zone in one direction, a line scan test can be also used (Ref 3).

Collected beads, or more precisely overlapped beads obtained by passing the torch for a given number of times at the same position, give relevant information on the heat treatment of particles (Ref 28, 29) by considering the central part and edges of the beads.

Coatings are analyzed by conventional methods [x-ray diffraction (XRD), optical microscopy (OM), scanning electron microscopy (SEM), field emission gun scanning electron microscopy (FESEM), transmission electron microscopy (TEM), energy dispersive spectroscopy (EDS), micro-hardness, etc.]. However, a difficult problem concerns the coating cross-sectioning and polishing, mostly due to their high toughness. A problem is also pending (and answers will have to be found in the near future to further understand coating architecture and manufacturing mechanism), i.e., the characterization of coating void contents in the range of few hundreds of nanometers. Indeed, image analysis coupled to stereological protocols, a very commonly implemented technique to characterize the void content level of micrometer-sized coatings manufactured by conventional plasma spraying, cannot be used anymore to quantify SPS coating void contents. This is due to the too low resolution of SEM pictures (one to two orders of magnitude lower than the characteristic dimension of voids), besides the recurrent problem of artifacts generated during polishing (pull-outs, scratches, etc.) that is even more emphasized on SPS coatings due to their higher resistance to abrasion. Mercury intrusion porosimetry (MIP) is also widely implemented to address the void content of plasma sprayed coatings, among them SPS ones, but this technique considers only open voids and the sample volume required for "high" measurement accuracy is far bigger than the volume of SPS coatings usually manufactured. USAXS and He pycnometry combined together have proven to be adapted techniques to quantify void size distribution, the total void content, and the open void content of SPS YSZ coatings. However, the experience will have to be extended to other natures of coatings with, as primary limitation for USAXS, the strong absorption of

high-energy x-ray radiation by numerous ceramic materials requiring to limit the thickness of the analyzed samples in order to avoid a dramatic increase in the noise/signal ratio limiting the measurement accuracy. A collective effort is required from the community to develop, define, and precise adapted measurement techniques (i.e., fast, accurate, global, etc.) permitting to address the void content of SPS coatings.

3. Liquid Stream-Hot Gas Flow Interactions

3.1 General Remarks

As indicated earlier, liquid stream or drops fragmentation depends strongly upon Weber, *We*, and Ohnesorge, *Oh*, dimensionless numbers. Fragmentation starts for *We* > 14 and can be delayed if *Oh* increases.

In axial liquid injection, the stream and the drops are directly injected in hot gases and are rapidly fragmented in tiny droplets (a few micrometers in diameter) that are then vaporized. In radial injection, the stream or the drops first encounter gases flowing in the periphery (fringes) of the hot core of the flame or plasma where velocities are high enough to fragment them and vaporize the liquid phase of the resulting droplets, but not sufficient enough for particles in suspension to be adequately heated or solution precursors to be pyrolyzed. Such poorly treated materials will be partially deposited in bead edges and thus incorporated into the coating, forming stacking defects.

Once drops and stream are fragmented into droplets of a few micrometers, they are vaporized. The fragmentation time is about two to three orders of magnitude shorter than that of vaporization (Ref 30). Thus, the fast vaporization of the liquid and the resulting gases cools down the hot gas flow drastically (Ref 30). This means hence that due to both the cooling of the hot gas flow and the low inertia of the sub-micrometer or nanometer sized particles (Ref 31), the spray distance has to be shorter than that in conventional spraying, i.e., 30-50 mm against 100-120 mm for conventional plasma spraying (Ref 31) and 60-90 mm with axial liquid injection HVOF against 200-300 mm for conventional HVOF spraying (Ref 15). Correspondingly, the heat flux imposed by the hot gas flow to the coating and substrate can be up to one order of magnitude higher than in conventional spraying.

Drop penetration is quite similar to that observed in conventional spraying: the particle momentum (here the drop or the stream) must be about the same as that imparted to it by the hot gas flow. However, if the particle size does not vary in conventional thermal spraying, it is not the case with liquid injection where the stream and drops are continuously fragmented upon their penetration in the jet. Consequently, the momentum density of the initial stream or drops $\rho_\ell v_\ell^2$ must be very large compared to that of the hot gas flow varying along the droplet trajectories.

According to the importance of the hot gas flow momentum density, it is of primary importance to avoid its variation with arc root fluctuations in plasma spraying. For example, for a constant arc current intensity when the voltage varies between 40 and 80 V, ρv^2 at the nozzle exit axis varies about 820% (Ref 31). Of course, the injection velocity for axial injection is probably less critical but the momentum density of the liquid stream must be high enough to achieve the penetration of the liquid within the hot gas flow.

At last, according to the drastic importance of the liquid momentum density, the atomization processes resulting in drops of different sizes and velocities do not appear to be necessarily well adapted to achieve the optimum penetration of the liquid.

3.2 Solutions

Once the solvent is selected (water, ethanol, isopropanol etc.), the solution concentration can be varied up to the (equilibrium) saturation concentration. For example, Chen et al. (Ref 16) have compared two solutions with aqueous salts containing zirconium and yttrium: one close to the saturation concentration (with 2.4 mole L^{-1}) and the other four times lower (0.6 mole L^{-1}). In the latter case and upon heating, the solvent evaporates and the solute precipitates at the surface for the low concentration, resulting in shell morphology. On the contrary, with a high concentration, precipitation starts at the surface but has the highest probability of propagating to the center if the droplet is small enough. The particles undergoing shell formation form bubble-like morphologies while those with volume formation result in molten particles and splats. Increasing the solution concentration does not modify the surface tension but it increases its viscosity, resulting in a better penetration of the liquid in the plasma jet (Ref 16).

3.3 Suspensions

The selection of the particles (morphology and size distributions) and their mass load in the suspension are key parameters. Typical mass loads vary between 5 and 20 wt.%, corresponding to typical equivalent solid feed rate of 1 to 6 g min^{-1} when considering ceramic materials of density 3-6 (Al_2O_3, ZrO_2, etc.). However, with a conventional plasma spray torch, coatings manufactured with a suspension with a particle mass load over 10% are less cohesive (Ref 3) (due very likely to the loading effect on the plasma flow), unless the warm gas enthalpy is increased.

The size distribution is also an important parameter to consider and the Stokes number (see Eq 1) has to be taken into consideration: the minimum size depends strongly upon the velocity imparted to the particles by the hot gas flow. For example, velocities such as those measured by Oberste-Berghaus et al. (Ref 13) with a Mettech Axial III torch and reaching 700 m s^{-1} allow using particles 3 times smaller than those whose average velocity is 233 m s^{-1}. Typically, particle sizes below 100 nm require very high velocities to avoid particles following the flow impacting the substrate and not striking the substrate.
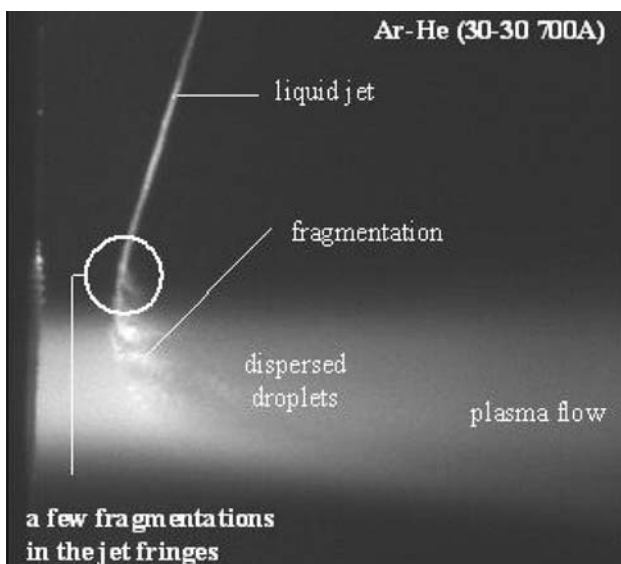
Moreover, the smaller the particles, the lower their inertia (Ref 32).

At last, as in conventional thermal spraying, the particle size distribution must be rather narrow. Agglomerations of particles must be avoided (Ref 32), which can be achieved for example by attrition or ball milling the suspension after its preparation.

3.4 Droplets and Particle Trajectories

Drops or liquid stream that have penetrated within the hot gas flow are fragmented in progressively smaller droplets which are widely dispersed within the jet, as shown in Fig. 1. Once the liquid phase is completely vaporized, particles (solid in suspension or solute shells or spheres in solutions) contained in each droplet will follow different trajectories where they will be heated and accelerated by the hot gas flow, their initial velocity is that of their ''mother'' droplet. Of course, particles probably agglomerate upon complete vaporization of liquid phase, as the size of individual lamellae collected onto substrates seems to indicate in some cases (Ref 32). In some other cases, those agglomerates seem to desegregate during their flight or are not formed, as the collection of single resolidified spheres onto substrates tends also to indicate. Obviously, some additional studies are required to further document the organization of the particles upon complete liquid phase vaporization. For example, in conventional plasma spraying, such initial velocities are in the range 100-150 m s^{-1}. Moreover, as shown in Fig. 2, when these small particles encounter high-temperature gradients along their trajectory, they are subjected to thermophoresis effect (Ref 3) that tends to eject them towards colder areas where they cool down.
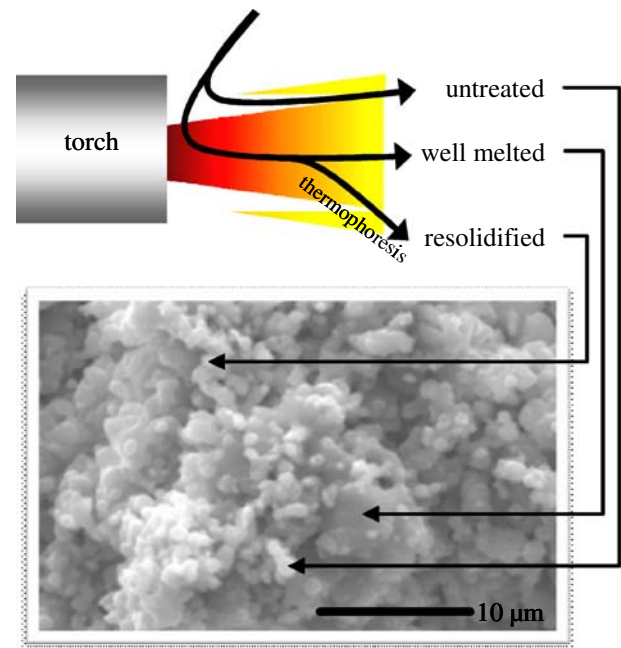
With axial injection of suspensions and due to turbulences, droplets are dispersed everywhere, including in the cold boundary layer of the flow. Thermophoresis effect also takes place.

## 4. Coating Manufacturing Mechanisms

4.1 Spray Beads

The degree of melting of particles can be evaluated with a line-scan-spray experiment considering either a simple bead in one passage or overlapped beads with successive passes (Ref 28). The bead thickness depends upon the relative torch to substrate velocity, the number of passes, the suspension or solution flow rates and the injection parameters, the mass loading of powder particles in suspension or the solution concentration and, of course, the torch operating conditions. A typical bead, manufactured by suspension plasma spraying, is presented in Fig. 3 together with the schematic of the torch movement. It can be seen that the bead can be fitted rather well with a Gaussian profile. Similar beads were obtained by Xie et al. (Ref 28).

Xie et al. (Ref 28) and Chen et al. (Ref 16) have studied the beads obtained with YSZ solutions and a conventional plasma spray torch under various operating conditions. The beads can be divided into adherent deposit and powdery deposit corresponding respectively to particles traveling in the warm or cold regions of the plasma jet. Adherent deposits seem to result from precursors traveling in both the warm and cold regions, the poorly treated precursor issued from the cold regions being incorporated

Fig. 1 Interaction of zirconia suspension drops (ethanol with 8 wt.% particles) with an Ar-He plasma jet (30 L/min Ar, 30 L/min He, 700 A, nozzle i.d. 6 mm). Picture taken with a laser flash (1 μs duration)

**Fig. 2** Schematic of particle trajectories within the warm gas flow with the corresponding coating
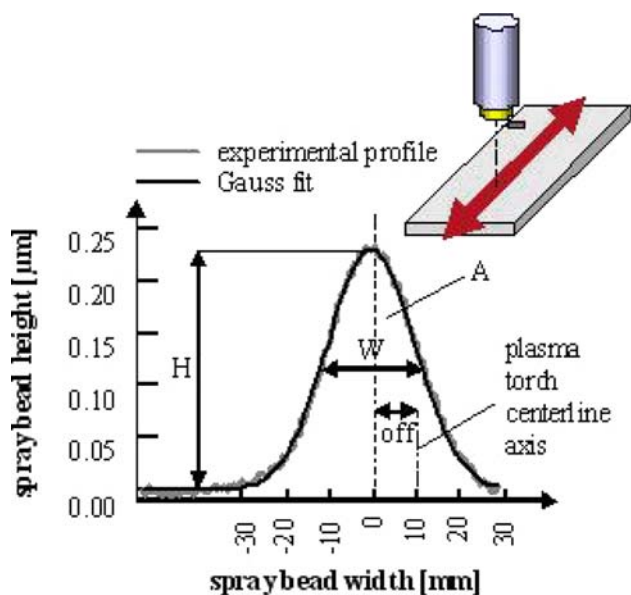
Fig. 3 Typical spray bead manufactured by suspension plasma spraying with the schematic of the corresponding torch movement

Fig. 4 Al_2O_3 spread bead obtained when spraying a suspension (α-Al_2O_3 powder feedstock of 1.3 μm average diameter dispersed in Et-OH) with an Ar-He d.c. plasma torch [F4-type plasma torch, Ar-He (30-30 L min^{-1}), arc current intensity of 600 A, anode i.d. at exit of 6 mm]

into the adherent deposit. Powdery deposits at the edges of the spray bead correspond to precursors traveling in the low-temperature regions (fringes).

Chen et al. (Ref 16) have studied the influence of the precursor concentrations. The central part of the spray bead deposited on a cold substrate consists of semi-pyrolyzed material that will form soft and porous coatings. The shells on droplet surfaces fracture and form bubbles upon impacting the substrate at room temperature. However, bubbles evolve to spongy deposits when the substrate temperature is raised to 450 °C. The high concentration precursor experiences volume precipitation, leading to fully melted lamella microstructure and dense coating. In both cases, non-pyrolyzed materials are pyrolyzed at the substrate surface and form aggregates when the substrate temperature is above the precursor pyrolysis temperature. This pyrolysis also occurs when reheating the coating by the successive torch passes (Ref 29).

A similar observation can be made when considering the spray beads obtained with suspensions (Fig. 4). The central part of the bead is relatively dense and comprises mainly a few splats, spherical particles, and unmelted ones. It corresponds to particles that have been well treated in the plasma core plus particles that have traveled in colder zones. At mid-height in the bead, the coating is less dense with many unmelted particles. At the edges of the bead, the coating is fully powdery. To our knowledge, no bead was studied in the works devoted to axial injection (Mettech plasma torch or HVOF torches).

It is also interesting to study the influence of the spray parameters on the bead morphology. This is illustrated in Fig. 5 depicting the influence of the spray distance and the mass load fraction of the particles. The densest coating is obtained at a spray distance of 30 mm (when the plasma
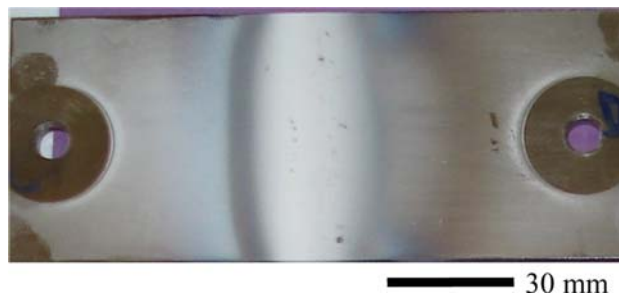
heat flux reaches 15 MW m^{-2}). The coating density seems to be slightly lower with the 10 wt.% mass load compared to the 5 wt.% one. The coating thickness, when the spray time is doubled, is also slightly decreased (due to the loading effect). When spraying at 40 mm, beads are thicker but less dense (due to the incorporation of more untreated particles).

4.2 Coatings

As discussed in the previous section, when superposing beads during spraying, some non-pyrolyzed particles (SPTS) or poorly treated particles (STS) are embedded in the coating during deposition. In SPTS, the amount of non-decomposed precursor can be controlled by spray parameters, primarily droplet injection momentum density, spray droplet size dispersion as well as precursor concentration (Ref 29). Upon heat exposure either by plasma torch passes or post-processing treatment, the pyrolysis of the non-pyrolyzed precursors generates tensile stresses driving the formation of cracks perpendicular to substrate surface ("vertical" cracks). When adapting the spray parameters to reduce the amount of non-pyrolyzed particles, dense (88%) YSZ coatings can be achieved as illustrated in Fig. 6.

In HVOF or plasma suspension spraying, it is crucial to achieve particles melting, or close to melting state, at impact. Thus, when using water instead of ethanol as suspension liquid phase, resulting coatings are generally more porous than those achieved with ethanol (Ref 3, 15, 33, 34). In the following, only results obtained with yttria-partially stabilized zirconia (Y-PSZ) solution or suspension plasma spraying will be presented.

Figure 7 depicts coatings obtained in one pass with two different Y-PSZ powders: Unitec 0.01 (Unitec Ceram, Stafford, UK) fused and crushed ($d_{10} = 0.05$, $d_{50} = 0.06$, and $d_{90} = 0.29$ μm) and Marion (Marion Technologies, Bordeaux, France), prepared by a soft chemical route ($d_{10} = 0.03$, $d_{50} = 0.06$, and $d_{90} = 0.88$ μm).

Both coating architectures are similar, with the coating obtained with fused and crushed particles being slightly thicker (15 μm against 12 μm in the same spray conditions). It can also be observed at the surface of both
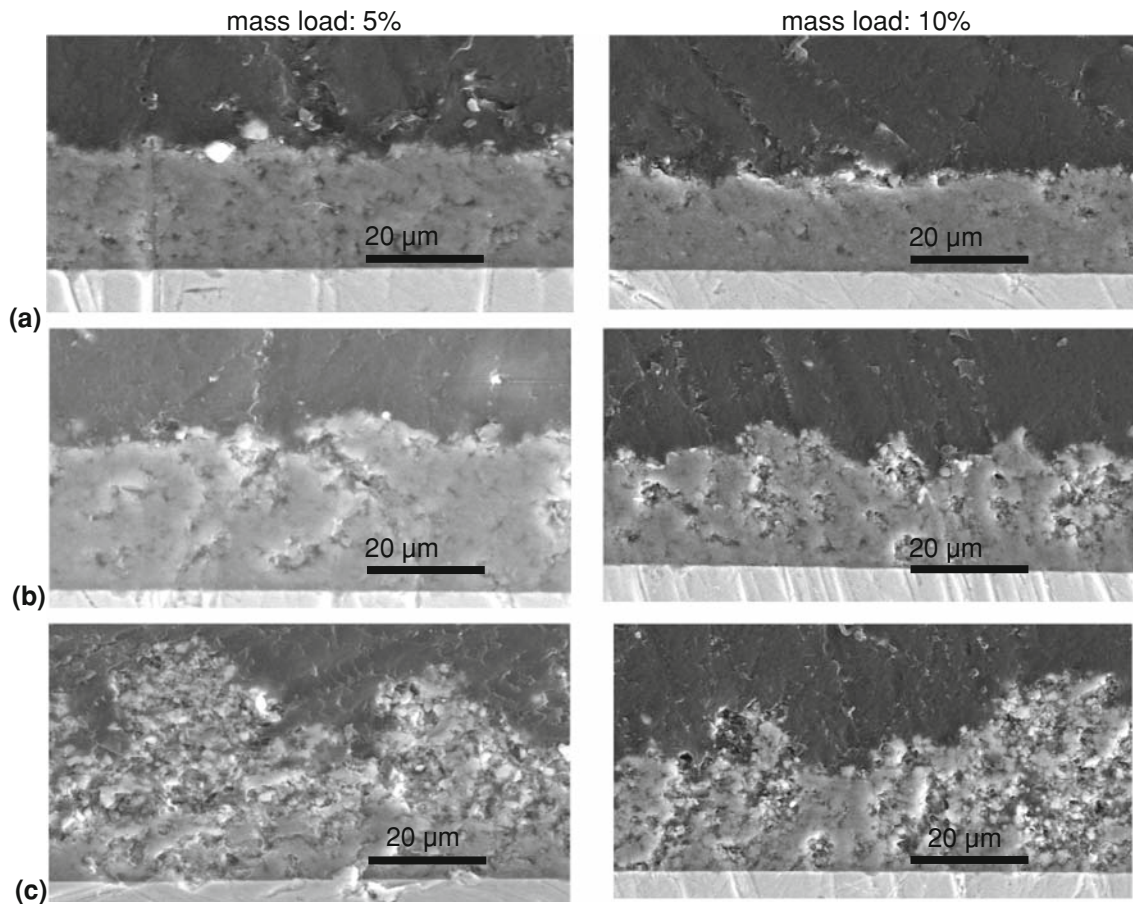
Fig. 5 Cross section of the beads along their axes for three spray distances (a, 30; b, 40; and c, 50 mm) and two particles mass loads [α-Al$_2$O$_3$ powder feedstock of 1.3 μm average diameter dispersed in Et-OH, 5 wt.% with 8 min spraying time and 10 wt.% with 4 min spraying time, F4-type plasma torch, Ar-He (30-30 L min^{-1}), arc current intensity of 600 A, anode i.d. at exit of 6 mm]

coating deposition of rather porous material (poorly melted particles) which seems to stick to the denser part of each pass.

When superimposing passes, as shown in Fig. 8(a), the different passes are clearly separated by porous layers that seem to induce porosities and delaminations in the upper layer. The probable explanation is depicted in Fig. 9 showing how, according to the spray pattern, the poorly treated particles traveling in the jet fringes are deposited at the surface of the warm previous pass, where most of them stick. The following well-melted particles, which have traveled in the warm zone of the plasma, form the next pass on the powdery layer deposited by the preceding particles traveling in the jet fringes. It is worth noting that for the first pass where the substrate temperature is below 500 K, almost no sticking of poorly treated particles occurs and the substrate/first pass interface is relatively clean compared to that between successive passes. When considering spray conditions with a highly fluctuating plasma jet ($\Delta V/V \sim 1$ with the Ar-H$_2$ plasma against 0.25 with the Ar-He one), more powdery material is deposited between successive passes with higher pore level, as seen in Fig. 8(b). The situation becomes worst in terms of

poorly treated particles deposition when injecting the suspensions in the Ar-H$_2$ plasma with lower injection velocity, as shown in Fig. 8(c). When adapting the spray pattern, it is nevertheless possible to get rid of most of the powdery layer between passes and obtain rather thick and dense coatings, as illustrated in Fig. 10.

4.3 Coating Morphologies

In general, Y-PSZ lamellae collected on a substrate preheated over the transition temperature (~350 K for Y-PSZ on stainless steel, alumina, or super alloys) are identical to those obtained by conventional spraying (Ref 30). However, their equivalent diameters are generally between 3.0 and 0.2 μm with thicknesses varying between 300 and 60 nm. Their size depends upon the initial particle sizes and in general the flattening degree seems to be about 2 at the maximum for d.c. conventional spray torches (Ref 32). Moreover, no crack during quenching appears (see, e.g., Fig. 3 of Ref 3).

Fractures of sprayed coatings exhibit a first layer (a few micrometers thick) close to the metallic substrate with a columnar structure and the rest of the coating shows a
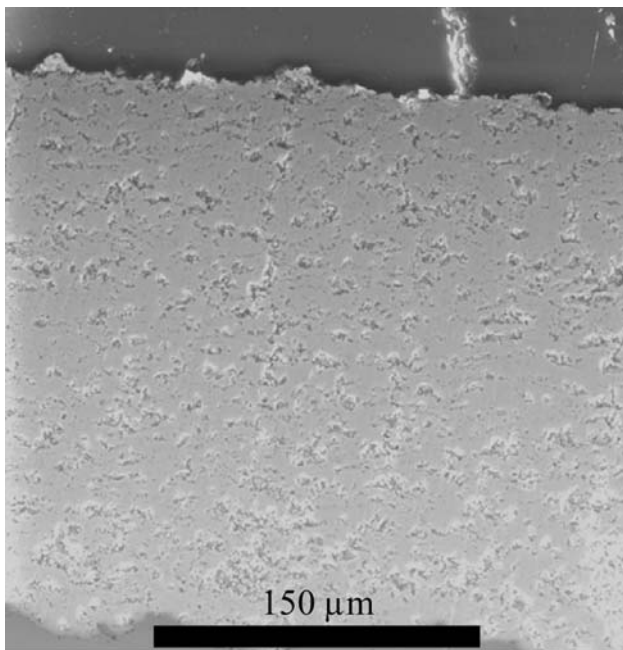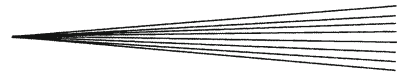
Fig. 6 Hard (1023 HV$_3$) and ''fairly'' dense (88%) YSZ obtained by achieving better melting. No crack perpendicular to substrate surface can be detected (Ref 24)

granular structures in which a few splats seem to be embedded (see Fig. 18 of Ref 32). A view of a Y-PSZ (8 wt.%) coating surface is presented in Fig. 11 with different magnifications. The coating surface presents some sort of ''cauliflower'' features with well-melted grains (spherical shape) and a few unmelted ones. This typical feature is confirmed by the cross-sectional views presented in Fig. 12.

At the moment, no clear explanations have been found for this unusual morphology. Works are in progress to determine if, after a few layers (a few micrometers thick), the thermal insulation together with the drastic heat flux from the plasma delays the lamella solidification. This situation could allow the surface tension force to take over, resulting in quasi-spherical particles in a molten state sticking together before their solidification.

When spraying solutions, the coatings from low concentration solutions are very porous and are composed of aggregated solid particles (Fig. 13a) while those obtained with high-concentration solutions are mainly composed of ultra-fine splats (Fig. 13b) (Ref 16). As shown in Fig. 14(a), coatings resulting from low concentrations are very porous (about 62% average density values), whereas those resulting from high concentrations are denser (81% average density) as shown in Fig. 14(b) (Ref 16). In the first case, the hardness is 1.3 ± 0.17 GPa, whereas it reaches 4.2 ± 0.22 GPa in the second one.

5. Applications

Many works have been devoted to solution spraying of thermal barrier coatings (TBCs) (Ref 16, 21, 28, 29).
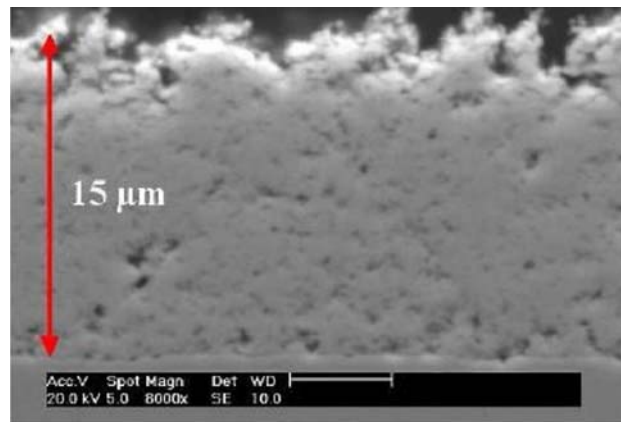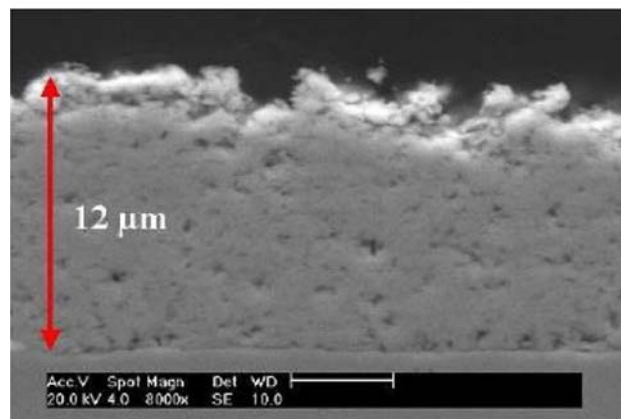

Fig. 7 Coatings manufactured with two different Y-PSZ powders: (a) fused and crushed Unitec 0.01 with $d_{50} = 0.06$ μm and (b) soft chemistry Marion with $d_{50} = 0.06$ μm. Both 20 wt.% suspensions were injected at 33.5 m s^{-1} in the same Ar-He plasma jet

As explained previously, the coatings contain uniformly distributed cracks, providing a high degree of strain tolerance to the ceramic topcoat. Compared to APS conventional TBCs, coatings produced by solution precursor plasma spray (SPPS) demonstrate (Ref 29) equal or greater durability, lower thermal conductivity than EB-PVD (electron beam physical vapor deposition) but higher than conventional APS coatings, higher in-plane toughness and bond strength.

Works have also been performed with suspensions [suspension plasma spraying (SPS) and high-velocity suspension fame spraying (HVSFS)] (Ref 11, 15, 17). For example, Kassner et al. (Ref 11) have obtained segmented coatings (7 cracks per mm following the coating cross section) for 300 μm thick coatings obtained by plasma spraying.

Ben-Ettouil et al. (Ref 33) nevertheless showed that resistances to isothermal and thermal shocks of Y-PSZ SPS coatings were higher for coatings exhibiting lower crack density, as depicted in Fig. 15.
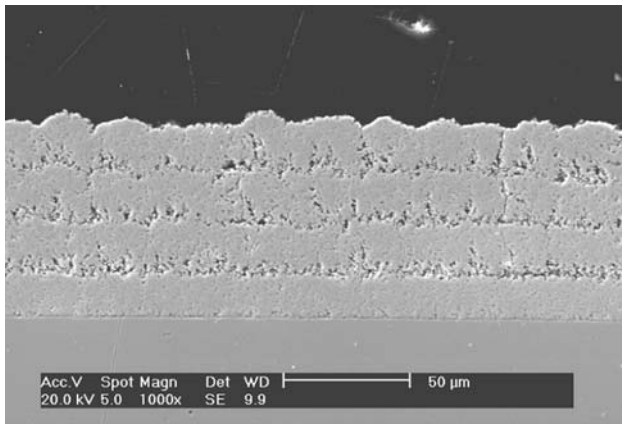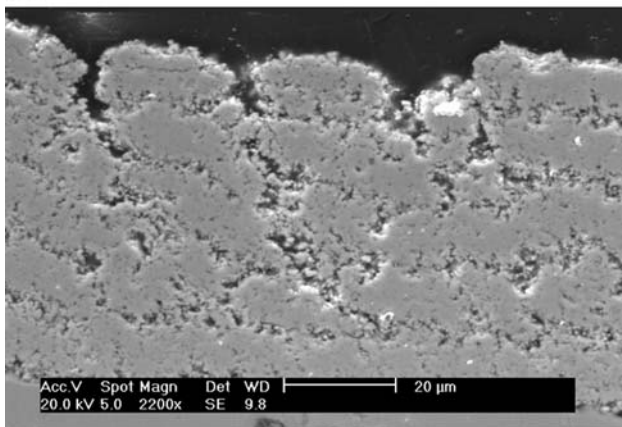
(a)
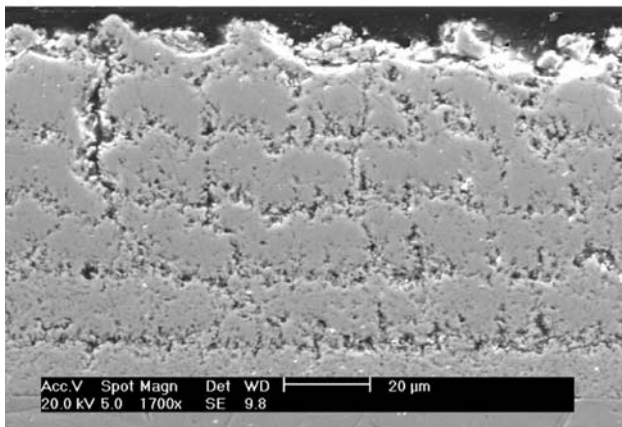
(b)

(c)

Fig. 8 Coatings (4-5 passes) obtained with the same Et-OH suspension (Unitec 0.02, fused and crushed $d_{50} = 0.39$ μm) sprayed under different operating conditions with a PTF4 torch (nozzle i.d. 6 mm). (a) Ar-He (30-30 L/min, 700 A, $v_{inj} = 33.5$ m s^{-1}). (b) Ar-H$_2$ (45-15 L/min, 500 A, $v_{inj} = 33.5$ m s^{-1}). (c) Ar-H$_2$ (45-15 L/min, 500 A, $v_{inj} = 26.6$ m s^{-1})

Numerous works are in progress to develop by SPS thin coatings (~10-15 μm) of Y-PSZ impervious to gases for the SOFC electrolyte. From works developed at SPCTS-University of Limoges (Ref 34), it appears that coating architecture is very sensitive to substrate roughness.
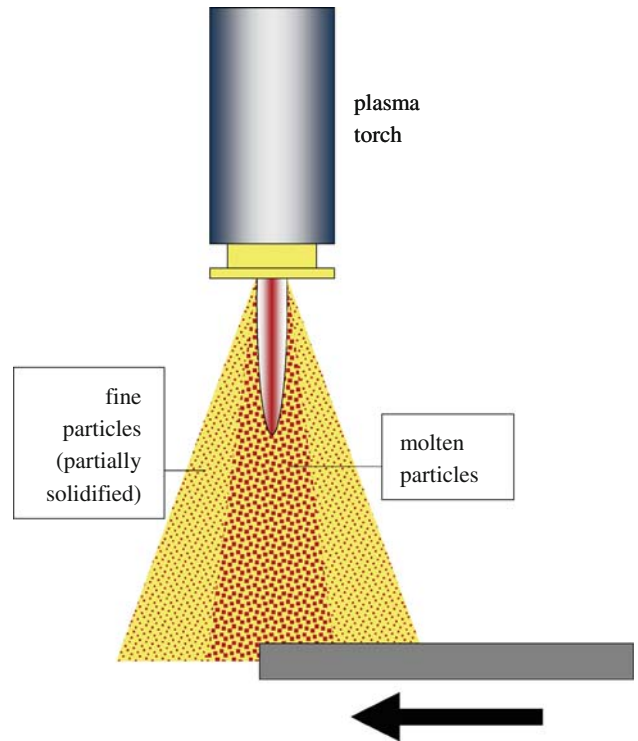

Fig. 9 Schematic explanation of the deposition on each pass of a powdery layer due to the sticking of poorly treated particles in the jet fringes preceding the well-melted particles deposition
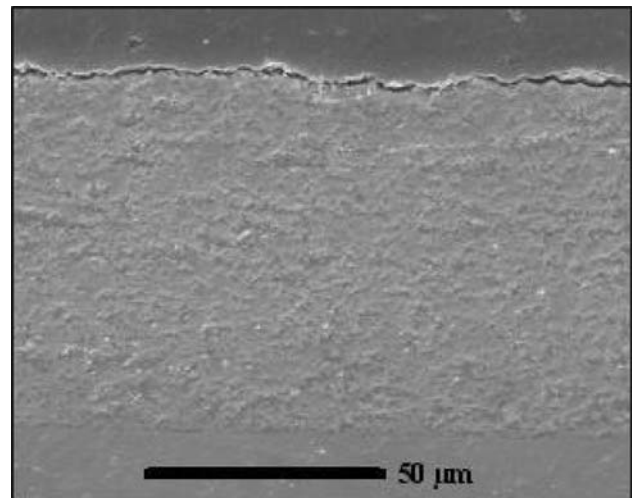

Fig. 10 Dense and thick Y-PSZ (8 wt.%) coating deposited with an Ar-He plasma, an injection velocity of 33.5 m s^{-1} and a suspension of Unitec 01 particles ($d_{50} = 0.06$ μm), the spray pattern being adapted to avoid powdery layers between passes

Indeed, large columnar stacking defects develop through the coating when the substrate surface roughness is higher than the average diameter of the feedstock particle, as depicted in Fig. 16. Reducing the stacking defects to enhance gas tightness (hermeticity) requires spraying onto smooth polished substrates.
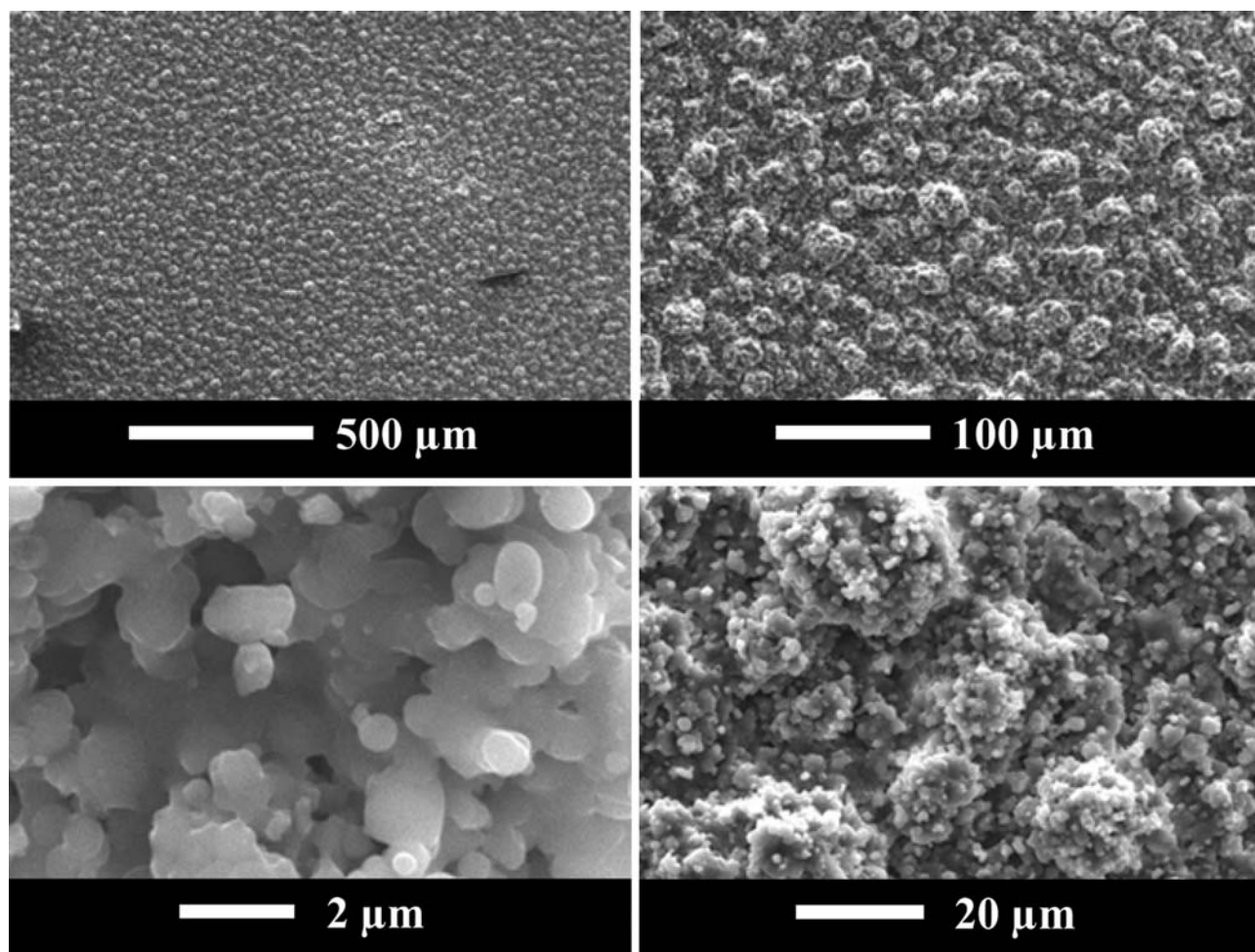
Fig. 11 Top view of an Y-PSZ suspension plasma sprayed coating [Unitec 0.1 particles, Ar-He plasma gas mixture (30-30 L min^{-1}), arc current intensity of 600 A, anode i.d. at exit of 6 mm] with four different magnifications
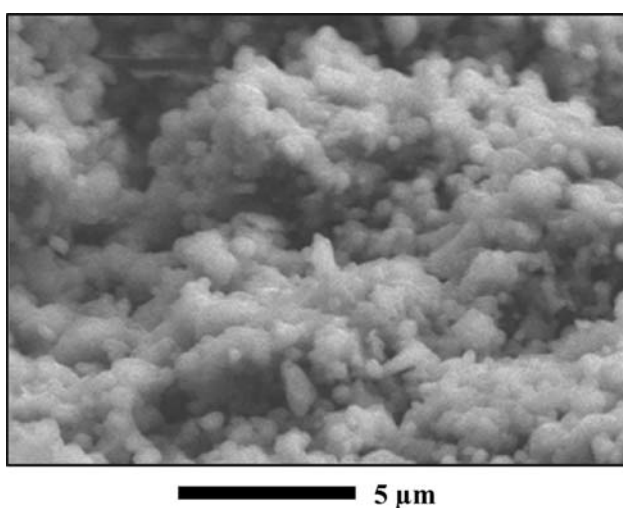

Fig. 12 Fractured cross sections of the coating presented in Fig. 11

Besides, Kassner et al. (Ref 11) have sprayed LSM $((La_{0.65}Sr_{0.3})MnO_3)$ and Y-PSZ to produce functional layer for SOFC cathodes using two injectors. According to the small particle size, such coatings should provide a higher amount of triple-phase boundaries.

Titania has been sprayed either by SPS (Ref 19, 22, 35, 36) or HVSFS (Ref 2, 15), or SPPS (Ref 36). TiO_2 coatings are mostly designed for photo-catalytic applications. Coatings sprayed with Et-OH base suspensions contained only 23% of anatase ratio (against 82 vol.% in the feedstock powder) and ensured a very low photo-catalytic decomposition of nitrogen oxides (Ref 37). On the contrary, with water base suspensions, the anatase phase and crystallites size were preserved and the conversion rate of pollutant reached 40% against 32% for the starting powders (Ref 22).

Using solution spraying (Ref 38), it was shown that when increasing the concentration, the anatase phase content decreases and the rutile phase increases. In fact, the formation of crystalline anatase and rutile phases in
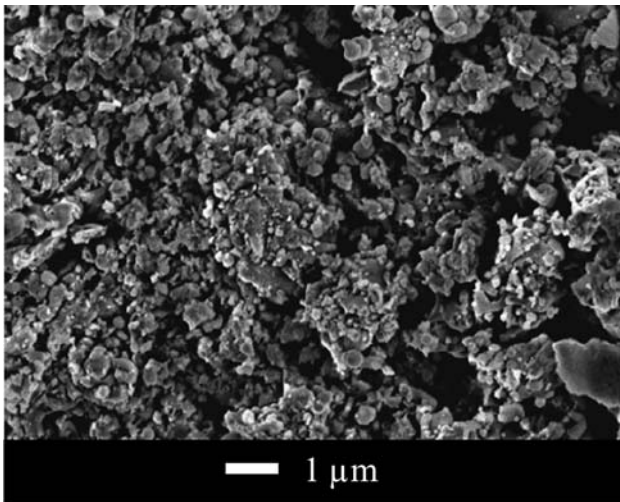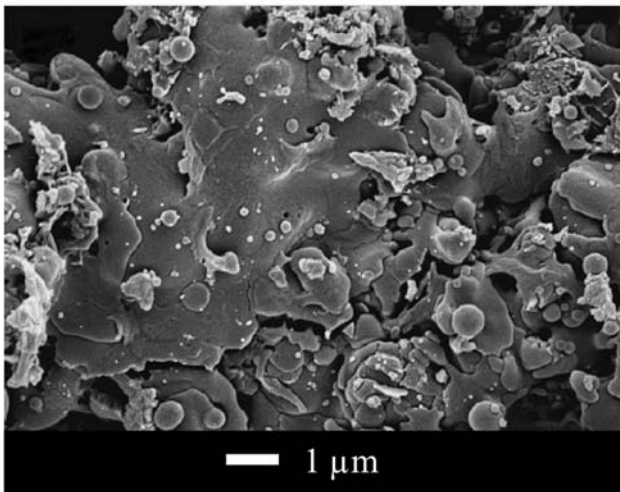
Fig. 13 Coating surface morphologies from solution precursors: (a) low concentration and (b) high concentration (Ref 16)

the as-sprayed coatings is the result of plasma flow heat treatment on the gel-like deposit (many non-pyrolyzed droplets).

The development of multilayer coatings of hydroxy-apatite (HA) and TiO_2 onto titanium substrate was studied by suspension plasma spraying (Ref 39). Two types of coatings were tested: duplex and graded coatings. The density of coating was improved as well as their cohesion when increasing the torch power level but unfortunately the HA was partially decomposed.

HA ethylene glycol based suspension was HVSFS processed (Ref 15) with 13 wt.% of HA powder, resulting in dense coatings structure with a porosity of about 1% (coating thickness 50 µm). Coatings consist of about 90% of HA with a small amount of tri-calcium-phosphate.

A phosphorous containing biocompatible glass was HVSFS processed also (Ref 15): coatings displayed a certain porosity that seemed to consist mainly of closed pores with some transverse micro-cracks.
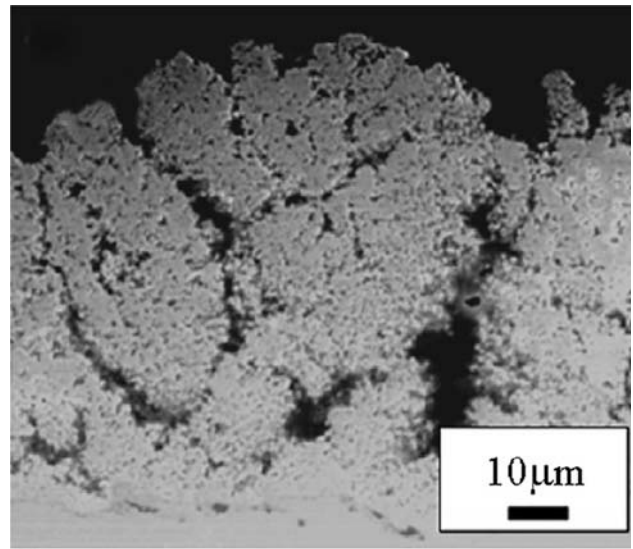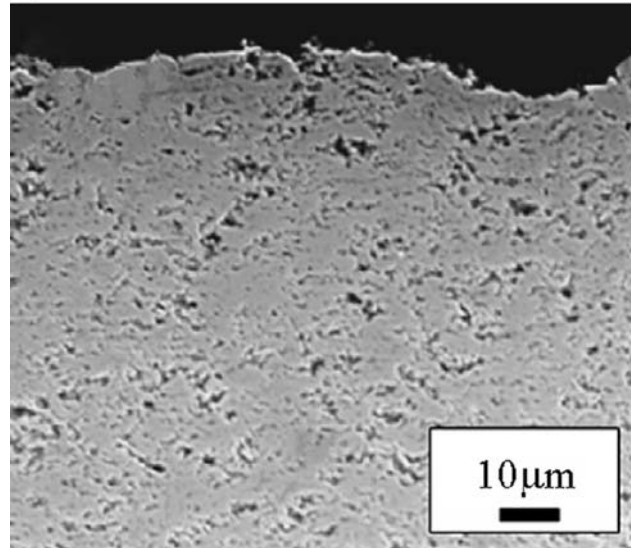

Fig. 14 Polished cross sections of coatings from solution precursors: (a) low concentration and (b) high concentration (Ref 16)

A CaO-ZrO_2-SiO_2 glass frit was processed by HVSFS (Ref 40). Such glass, if dense, should have excellent anti-corrosion properties on metal or ceramic substrates. The coatings obtained were much denser than those formerly investigated and plasma sprayed. Some problems were connected to the formation of molten glass deposits in the combustion chamber and their subsequent embedment in the coating. Work is in progress to overcome this problem to achieve dense coatings with strong inter-lamellae cohesion.

WC-Co coatings were deposited using an axial injection plasma torch and an Et-OH suspension of sub-micrometer-sized feedstock powders (Ref 13). With a proper selection of spray parameters, porosities below 0.2% were achieved with hardness over 700 HV_{3N}. The best coatings

(a)   (b)

after 10 thermal cycles
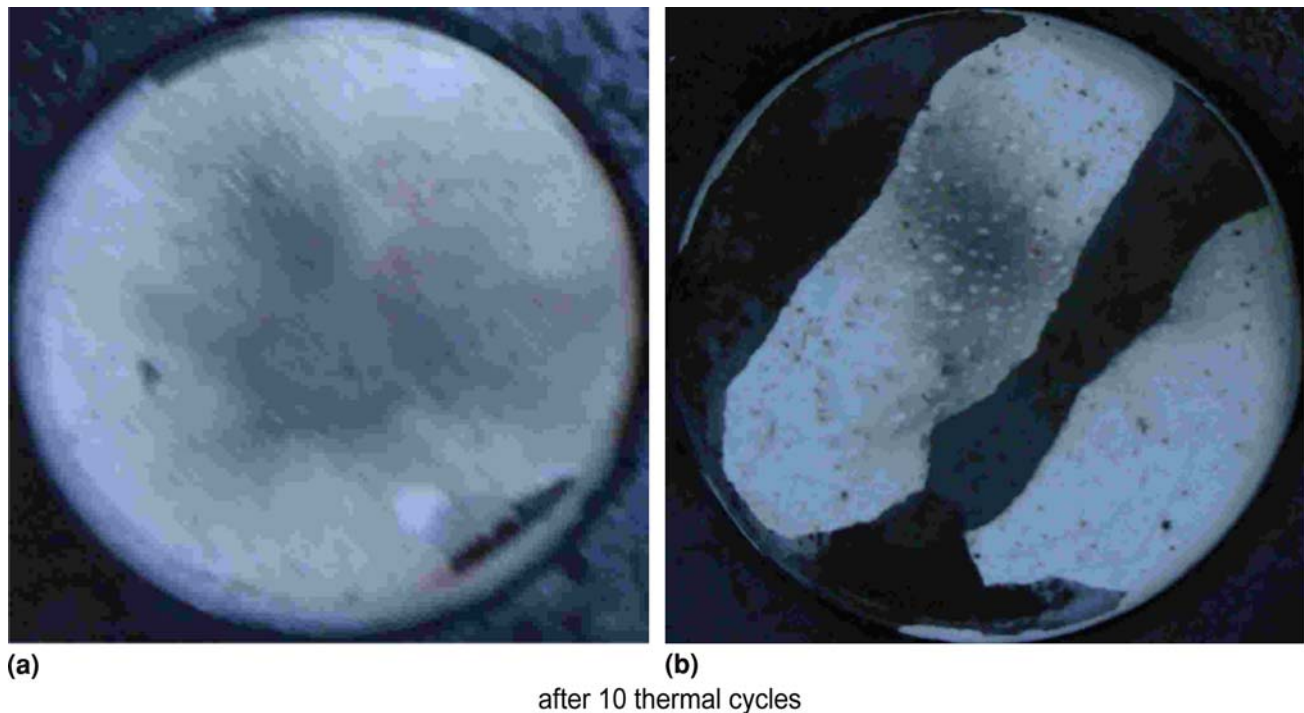
Fig. 15 Resistance to thermal shocks of SPS Y-PSZ coatings (about 100 μm thick) with a thermal flux of 0.5 MW m^{-2} applied until the substrate/coating interface temperature reaches 850 °C. Cooling is ensured down to 50 °C by compressed air flow. (a) Coating with low density of cracks and (b) coating with a higher density of cracks
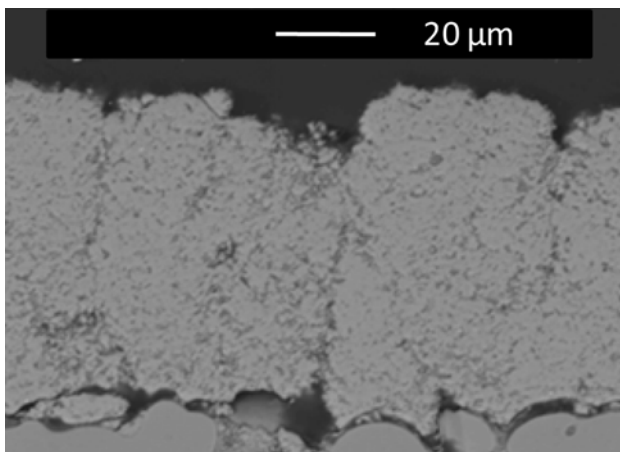
Fig. 16 Y-PSZ coating sprayed onto a substrate exhibiting an average substrate roughness 40 times higher than the feedstock particle average diameter: columnar stacking defects develop through the coating thickness

corresponded to the highest particle velocities (~800 m s^{-1}) and lowest temperature (at the minimum, 2200 °C). It seems that the measured carbon loss in the carbide is principally associated to deposition of layers of highly oxidized overspray. The properties of the feedstock powder and feed suspension play a critical role in the resulting coatings quality.

Alumina coatings were sprayed by Toma et al. using SPS and HVSFS (axial injection) spraying (Ref 35).

The initial mean particle diameter was 0.3 μm and either water or Et-OH was used for the suspension. Et-OH base suspension spraying with Ar-H$_2$ plasma forming gas mixture resulted in 18.9 ± 2.5% porosity against 11.6% with an Ar-He plasma. With HVSFS (acetylene-oxygen) and an aqueous suspension, the porosity was 7.6 ± 2.8%.

Darut et al. (Ref 41) compared the tribological properties of alumina coatings structured at two different scales, a micrometer one (d_{50} of particle size distribution of 36 μm) manufactured by APS and a sub-micrometer one (d_{50} of particle size distribution of 0.4 μm) manufactured by SPS. Coatings architectures were analyzed and their friction coefficient and wear rate in dry sliding mode were measured in ball-on-disk friction conditions (α-Al$_2$O$_3$ ball of 6 mm in diameter). The friction coefficient of Al$_2$O$_3$ coatings was decreased by a factor of two (0.4 for SPS layers to be compared to 0.8-0.9 for APS ones) when the structure scale was divided by two orders of magnitude, although alumina is not a material suitable for friction layers. Moreover, the wear rate was 30 times lower for SPS layers compared to the one of APS layers (Fig. 17).

Gadow et al. (Ref 2) have sprayed by HVSFS a mixture of Al$_2$O$_3$ (150 nm) and Y-PSZ (12 nm) dispersed in 30/70 wt.% isopropanol/water mixtures with a 20 wt.% solid content. The coatings reveal that nano-sized particles of zirconia are embedded in an alumina matrix. The spray conditions were tailored to achieve complete alumina melting with the zirconia particles remaining solid. As the time between melting and reconsolidation is extremely short, the two components are almost immiscible.
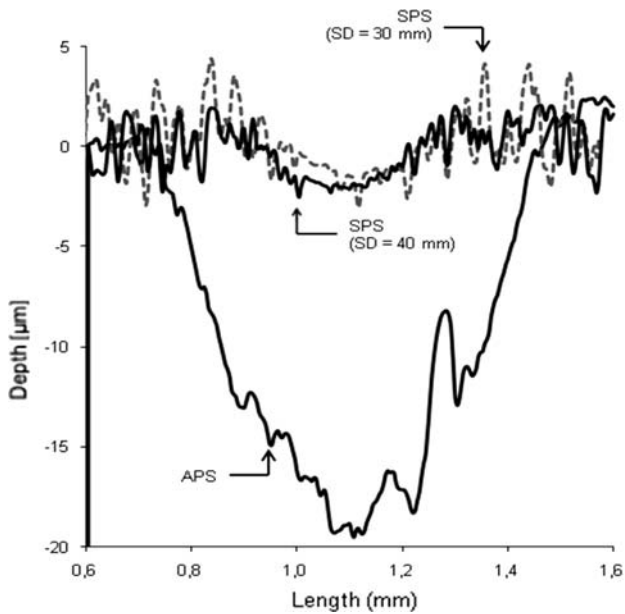
Fig. 17 Wear profiles for α-Al$_2$O$_3$ micrometer-sized (APS) and sub-micrometer-sized (SPS, spray distance = 30 and 40 mm) coatings (ball-on-disk friction test, α-Al$_2$O$_3$ ball of 6 mm in diameter, 2 N load, relative speed of 0.1 m s^{-1} and sliding distance of 1500 m. The test was operated in the dry mode and the wear scraps were constantly removed by an air jet located behind the contact point)

Oberste-Berghaus et al. (Ref 12) have also deposited Al$_2$O$_3$-ZrO$_2$ coatings by SPS and HVSFS, both with axial injection. With optimized spray conditions, the smaller nano-sized particles create fine laminates of alumina and zirconia layers, while slightly larger particles promote pseudo-alloyed alumina-zirconia amorphous phase components. A large variety of microstructures and properties of suspension-sprayed Al$_2$O$_3$-ZrO$_2$ composites was introduced by the different feedstock, spray systems and operating conditions.

SPPS was used to spray 75% dense coatings of metastable ceramics in the ZrO$_2$-10 mol.% Al$_2$O$_3$ binary system (Ref 42). The coating microstructure contains a rich variety of features and phases. Coatings are predominantly nano-structured (grain size < 100 nm) and made of tetragonal phase of ZrO$_2$ with Al^{3+} in solid solution.

The ternary systems (mol%) 10Al$_2$O$_3$-86.4ZrO$_2$-3.6Y$_2$O$_3$ and 20Al$_2$O$_3$-76.4ZrO$_2$-3.6Y$_2$O$_3$ were processed by SPPS (Ref 43). The nanostructures (10-40 nm) in both coatings were made predominantly of tetragonal (t) ZrO$_2$ phase with some cubic phase. The sub-micrometer-sized regions contain, in addition to t-ZrO$_2$, small amounts of crystalline Al$_2$O$_3$ phases. Thus, solution plasma spraying allows producing metastable ceramics with unusual structures.

6. Conclusion

Since about a decade, the interest to manufacture on large surfaces "thick" finely structured or nano-structured layers has been increasingly growing. If nano-structured architectures can be manufactured by gas condensation routes (CVD, PE-CVD, PVD, EB-PVD, etc.), their thicknesses can hardly be higher than a few micrometers. On the contrary, plasma spray coating thicknesses from 50 μm to a few millimeters are easily achieved but with no nano-structured architectures after particle melting.

This explains the interest for STS and SPTS, both allowing achieving finely structured layers of thicknesses varying between a few micrometers up to a few hundred of micrometers.

As the deposition rate can reach one-fifth to one-fourth of the one encountered in conventional plasma spraying, these techniques seem promising to manufacture dense or controlled porosity coatings and functionally graded layers. Nevertheless, compared to conventional thermal spraying, STS and SPTS are by far more complex because fragmentation and vaporization of the liquid control the processes.

Numerous studies are still necessary to reach a better understanding of the involved phenomena and for that the development of diagnostic techniques to quantify either the in-flight droplet or particle temperature and velocity or to visualize the droplets/plasma interactions must be improved or newly developed.

References

1. V. Viswanathan, T. Laha, K. Balani, A. Agarwal, and S. Seal, Challenges and Advances in Nanocomposite Processing Techniques, *Mater. Sci. Eng.*, 2006, **R54**, p 121-285
2. R. Gadow, F. Kern, and A. Killinger, Manufacturing Technologies for Nanocomposite Ceramic Structural Materials and Coatings, *Mater. Sci. Eng.*, 2008, **B148**, p 58-64
3. P. Fauchais, R. Etchart-Salas, V. Rat, J.-F. Coudert, N. Caron, and K. Wittmann-Ténèze, Parameters Controlling Liquid Plasma Spraying: Solutions, Sols or Suspensions, *J. Therm. Spray Technol.*, 2008, **17**(1), p 31-59
4. R.S. Lima and B.R. Marple, Thermal Spray Coatings Engineered from Nanostructured Ceramic Agglomerated Powders for Structural, Thermal Barrier and Biomedical Applications: A Review, *J. Therm. Spray Technol.*, 2007, **16**(1), p 40-63
5. F. Ben-Ettouil, O. Mazhorova, B. Pateyron, H. Ageorges, M. El-Ganaoui, and P. Fauchais, Predicting Dynamic and Thermal Histories of Agglomerated Particles Injected within a d.c. Plasma Jet, *Surf. Coat. Technol.*, 2008, **202**, p 4491-4495
6. D.J. Branagan, M. Breitsameter, B.E. Meacham, and V. Belashchenko, High-Performance Nanoscale Composite Coatings for Boiler Applications, *J. Therm. Spray Technol.*, 2005, **14**(2), p 196-204
7. D.J. Branagan, W.D. Swank, and B.E. Meacham, Maximizing the Glass Fraction in Iron-Based High Velocity Oxy-Fuel Coatings, *Met. Mater. Trans. A*, 2009, **40**(6), p 1306-1313
8. S. Basu, E.H. Jordan, and B.M. Cetegen, Fluid Mechanics and Heat Transfer of Liquid Precursor Droplets Injected into High-Temperature Plasmas, *J. Therm. Spray Technol.*, 2008, **17**(1), p 60-72
9. K. Wittmann-Ténèze, K. Vallé, L. Bianchi, P. Belleville, and N. Caron, Nanostructured Zirconia Coatings Processed by PRO-SOL Deposition, *Surf. Coat. Technol.*, 2008, **202**, p 4349-4354
10. P. Fauchais, V. Rat, J.-F. Coudert, R. Etchart-Salas, and G. Montavon, Operating Parameters for Suspension and Solution Plasma-Spray Coatings, *Surf. Coat. Technol.*, 2008, **202**, p 4309-4317
11. H. Kassner, R. Siegert, D. Hathiramani, R. Vassen, and D. Stoever, Application of Suspension Plasma Spraying (SPS) for Manufacture of Ceramic Coatings, *J. Therm. Spray Technol.*, 2008, **17**(1), p 115-123

12. J. Oberste-Berghaus, J.-G. Legoux, C. Moreau, F. Tarasi, and T. Chraska, Mechanical and Thermal Transport Properties of Suspension Thermal-Sprayed Alumina-Zirconia Composite Coatings, *J. Therm. Spray Technol.*, 2008, **17**(1), p 91-104

13. J. Oberste-Berghaus, B. Marple, and C. Moreau, Suspension Plasma Spraying of Nanostructured WC-12Co Coatings, *J. Therm. Spray Technol.*, 2006, **15**(4), p 676-681

14. A. Killinger, M. Kuhn, and R. Gadow, High-Velocity Suspension Flame Spraying (HVSFS), a New Approach for Spraying Nanoparticles with Hypersonic Speed, *Surf. Coat. Technol.*, 2006, **201**, p 1922-1929

15. R. Gadow, A. Killinger, and J. Rauch, New Results in High Velocity Suspension Flame Spraying (HVSFS), *Surf. Coat. Technol.*, 2008, **202**, p 4329-4336

16. D. Chen, E.H. Jordan, and M. Gell, Effect of Solution Concentration on Splat Formation and Coating Microstructure Using the Solution Precursor Plasma Spray Process, *Surf. Coat. Technol.*, 2008, **202**, p 2132-2138

17. R. Rampon, C. Filiatre, and G. Bertrand, Suspension Plasma Spraying of Y-PSZ Coatings: Suspension Atomization and Injection, *J. Therm. Spray Technol.*, 2008, **17**(1), p 105-114

18. R. Rampon, F.-L. Toma, G. Bertrand, and C. Coddet, Liquid Plasma Sprayed Coatings of Yttria-Stabilized Zirconia for SOFC Electrolytes, *J. Therm. Spray Technol.*, 2006, **15**(4), p 682-688

19. R. Jaworski, L. Pawlowski, F. Roudet, S. Kozerski, and A. Le Maguere, Influence of Suspension Plasma Spraying Process Parameters on TiO$_2$ Coatings Microstructure, *J. Therm. Spray Technol.*, 2008, **17**(1), p 73-81

20. A. Ozturk and B.M. Cetegen, Morphology of Ceramic Particulates Formed in a Premixed Oxygen/Acetylene Flame from Liquid Precursor Droplets, *Acta Mater.*, 2005, **53**, p 2531-2544

21. L. Xie, D. Chen, E.H. Jordan, A. Ozturk, F. Wu, X. Ma, B.M. Cetegen, and M. Gell, Formation of Vertical Cracks in Solution-Precursor Plasma-Sprayed Thermal Barrier Coatings, *Surf. Coat. Technol.*, 2006, **201**, p 1058-1064

22. H. Podlesak, L. Pawlowski, J. Laureyns, R. Jaworski, and T. Lampke, Advanced Microstructural Study of Suspension Plasma Sprayed Titanium Oxide Coatings, *Surf. Coat. Technol.*, 2008, **202**, p 3723-3731

23. R. Rampon, O. Marchand, C. Filiatre, and G. Bertrand, Influence of Suspension Characteristics on Coatings Microstructure Obtained by Suspension Plasma Spraying, *Surf. Coat. Technol.*, 2008, **202**, p 4337-4342

24. E.H. Jordan, M. Gell, P. Benzani, D. Chen, S. Basa, B. Cetegem, F. Wa, and X.C. Ma, *Thermal Spray 2007: Global Coating Solutions*, B.R. Marple, M.M. Hyland, Y.-C. Lau, C.-J. Li, R.S. Lima, and G. Montavon, Ed., ASM International, Materials Park, OH, 2007, p 463-467

25. P. Blazdell and S. Kuroda, Plasma Spraying of Submicron Ceramic Suspensions Using a Continuous Ink Jet Printer, *Surf. Coat. Technol.*, 2000, **123**(2-3), p 239-246

26. R. Etchart-Salas, V. Rat, J.-F. Coudert, P. Fauchais, N. Caron, K. Wittman, and S. Alexandre, Influence of Plasma Instabilities in Ceramic Suspension Plasma Spraying, *J. Therm. Spray Technol.*, 2007, **16**(5-6), p 857-865

27. C. Marchand, A. Vardelle, G. Mariaux, and P. Lefort, Modeling of the Plasma Spray Process with Liquid Feedstock Injection, *Surf. Coat. Technol.*, 2008, **202**, p 4458-4464

28. L. Xie, X. Ma, A. Ozturk, E.H. Jordan, N.P. Padture, B.M. Cetegen, D.T. Xiao, and M. Gell, Processing Parameter Effects on Solution Precursor Plasma Spray Process Spray Patterns, *Surf. Coat. Technol.*, 2004, **183**(1), p 51-61

29. M. Gell, E.H. Jordan, M. Teicholz, B.M. Cetegen, N. Padture, L. Xie, D. Chen, X. Ma, and J. Roth, Thermal Barrier Coatings made by the Solution Precursor Plasma Spray Process, *J. Therm. Spray Technol.*, 2008, **17**(1), p 124-135

30. J. Fazilleau, C. Delbos, V. Rat, J.-F. Coudert, P. Fauchais, and B. Pateyron, Phenomena Involved in Suspension Plasma Spraying Part 1: Suspension Injection and Behavior, *Plasma Chem. Plasma Process.*, 2006, **26**, p 371-391

31. R. Etchart-Salas, "Plasma Spraying of Suspensions of Sub-Micrometer Particles. Analytical and Experimental Approaches of the Phenomena Controlling the Reproducibility and Quality of Coatings," Ph.D. Thesis, University of Limoges, France, 2007 (in French)

32. C. Delbos, J. Fazilleau, V. Rat, J.-F. Coudert, P. Fauchais, and B. Pateyron, Phenomena Involved in Suspension Plasma Spraying Part 2: Zirconia Particle Treatment and Coating Formation, *Plasma Chem. Plasma Process.*, 2006, **26**, p 393-414

33. F. Ben-Ettouil, A. Denoirjean, A. Grimaud, G. Montavon, and P. Fauchais, *Sub-Micrometer-Sized Y-PSZ Thermal Barrier Coatings Manufactured by Suspension Plasma Spraying: Process, Structure and Some Functional Properties*, These Proceedings

34. E. Brousse, G. Montavon, P. Fauchais, A. Denoirjean, V. Rat, J.-F. Coudert, and H. Ageorges, Thin and Dense Yttria-Partially Stabilized Zirconia Electrolytes for IT-SOFC Manufactured by Suspension Plasma Spraying, *Thermal Spray Crossing Borders, June 2-4, 2008, Maastricht, The Netherlands*, E. Lugscheider, Ed., DVS, Düsseldorf, Germany, 2008, p 547-552

35. F.-L. Toma, L.-M. Berger, T. Naumann, and S. Langner, Microstructures of Nanostructured Ceramic Coatings Obtained by Suspension Thermal Spraying, *Surf. Coat. Technol.*, 2008, **202**, p 4343-4348

36. F.-L. Toma, G. Bertrand, S. Begin, C. Meunier, O. Barres, D. Klein, and C. Coddet, Microstructure and Environmental Functionalities of TiO$_2$-Supported Photocatalysts Obtained by Suspension Plasma Spraying, *Appl. Catal. B*, 2006, **68**, p 74-84

37. F.-L. Toma, G. Bertrand, S.-O. Chwa, C. Meunier, D. Klein, and C. Coddet, Comparative Study on the Photocatalytic Decomposition of Nitrogen Oxides Using TiO$_2$ Coatings Prepared by Conventional Plasma Spraying and Suspension Plasma Spraying, *Surf. Coat. Technol.*, 2006, **200**, p 5855-5862

38. D. Chen, E.H. Jordan, and M. Gell, Porous TiO$_2$ Coating using the Solution Precursor Plasma Spray Process, *Surf. Coat. Technol.*, 2008, **202**, p 6113-6119

39. R. Tomaszek, L. Pawlowski, L. Gengembre, J. Laureyns, and A. Le Maguer, Microstructure of Suspension Plasma Sprayed Multilayer Coatings of Hydroxyapatite and Titanium Oxide, *Surf. Coat. Technol.*, 2007, **201**, p 7432-7440

40. G. Bolelli, J. Rauch, V. Cannillo, A. Killinger, L. Lusvarghi, and R. Gadow, Investigation of High-Velocity Suspension Flame Sprayed (HVSFS) Glass Coatings, *Mater. Lett.*, 2008, **62**, p 2772-2775

41. G. Darut, H. Ageorges, A. Denoirjean, G. Montavon, and P. Fauchais, Effect of the Structural Scale of Plasma-Sprayed Alumina Coatings on Their Friction Coefficients, *J. Therm. Spray Technol.*, 2008, **17**(5-6), p 788-795

42. A.L. Vasiliev, N.P. Padture, and X. Ma, Coatings of Metastable Ceramics Deposited by Solution-Precursor Plasma Spray: I. Binary ZrO$_2$–Al$_2$O$_3$ System, *Acta Mater.*, 2006, **54**(18), p 4913-4920

43. A.L. Vasiliev, N.P. Padture, and X. Ma, Coatings of Metastable Ceramics Deposited by Solution Precursor Plasma Spray: II. Ternary ZrO$_3$-Y$_2$O$_3$-Al$_2$O$_3$ System, *Acta Mater.*, 2006, **54**(18), p 4921-4928